

SCIENTIFIC REPORTS



OPEN

Clear-cut observation of clearance of sustainable upconverting nanoparticles from lymphatic system of small living mice

Received: 05 March 2016

Accepted: 18 May 2016

Published: 06 June 2016

Hye Sun Park^{1,*}, Sang Hwan Nam^{2,*}, Jongwoo Kim², Hyung Seon Shin³, Yung Doug Suh^{2,4} & Kwan Soo Hong^{1,5,6}

The significance of lymphatic system has gathered great attention for immunotechnology related to cancer metastasis and immunotherapy. To develop innovative immunodiagnostics and immunotherapy in *in vivo* environments, it is very important to understand excretion pathways and clearance of injected cargoes. Herein, we employed Tm³⁺-doped upconverting nanoparticles (UCNPs) with versatile advantages suitable for long-term non-invasive *in vivo* optical imaging and tracking. Transport and retention of the UCNPs in the lymphatic system were evaluated with high-quality NIR-to-NIR upconversion luminescence (UCL) imaging. We obtained their kinetic luminescence profiles for the injection site and sentinel lymph node (SLN) and observed luminescence signals for one month; we also examined UCL images in SLN tissues, organs, and faeces at each time point. We speculate that the injected UCNPs in a footpad of a small mouse are transported rapidly from the lymphatic system to the blood system and then eventually result in an efficient excretion by the hepatobiliary route. These results will support development of novel techniques for SLN biopsy as well as immunotechnology.

The lymphatic system plays an important role in the diagnosis of cancer metastasis and immunotherapeutic responses in the human body^{1,2}. Lymph nodes are major organs in lymphatic system, acting as a protector from foreign materials and as a communicating area with confluent immune cells. The state of lymph node reflects the change of immune system against infections or diseases. Especially, it is important to identify the nearest lymph node (sentinel lymph node, SLN) to tumor tissue for diagnosis of cancer metastasis because cancer cells spread out through lymph node.

For sentinel lymph node (SLN) mapping and biopsy techniques, imaging probes containing fluorophores have been widely developed in view of accurate positioning with longer retention in SLN³⁻⁶. Organic fluorophores such as indocyanine green (ICG) have been applied in clinical use for SLN mapping and their modified nanomaterials have been studied to overcome their limits, rapid and extensive dispersion along the lymphatic flow which cause imprecise positioning of sentinel node^{3,4}. However, they may also give misleading results due to their biodegradation in *in vivo* environments and photobleaching from repeated exposure to light. In particular, in long-term *in vivo* imaging, the probes are desired to have photostability and signal uniformity to facilitate quantitative analysis from the obtained images and low *in vivo* toxicity even in the condition of long circulation.

Recently, lanthanide-doped upconverting nanoparticles (UCNPs) have gathered great attention because of their photostability and biocompatibility⁷⁻¹⁰. UCNPs are free from autofluorescence background and thus provide a high signal-to-noise ratio (SNR). In particular, near-infrared (NIR) emission of Tm³⁺-doped UCNPs facilitates highly sensitive detection (SNR > 30) with a large penetration depth (>2 cm) in biological tissues¹¹. It has been

¹Bioimaging Research Team, Korea Basic Science Institute, Cheongju 28119, Korea. ²Laboratory for Advanced Molecular Probing (LAMP), Research Center for Convergence NanoRaman Technology, Korea Research Institute of Chemical Technology, Daejeon 34114, Korea. ³Environmental Monitoring & Research Team, Korea Basic Science Institute, Cheongju 28119, Korea. ⁴School of Chemical Engineering, Sungkyunkwan University, Suwon 16419, Korea. ⁵Bioanalytical Science, University of Science and Technology, Daejeon 34113, Korea. ⁶Graduate School of Analytical Science and Technology, Chungnam National University, Daejeon 34134, Korea. *These authors contributed equally to this work. Correspondence and requests for materials should be addressed to Y.D.S. (email: ydsuh@kricr.re.kr) or K.S.H. (email: kshong@kbsi.re.kr)

reported that *in vivo* NIR imaging using Tm³⁺-doped UCNP could provide improved visualization in lymphatic imaging compared to UCNP-based visible or quantum dot (QD)-based fluorescence imaging^{12,13}.

One of the most overlooked factors in the study of lymphatic imaging using nanoprobes is their clearance after assuming roles. Recently, fluorescent NIR dye doped-silica nanoparticles were employed in a study of long-term *in vivo* SLN mapping in the lymphatic system, and efficient excretion from mice was demonstrated^{14,15}. However, long-term *in vivo* imaging and biodistribution study using UCNP in the lymphatic system have not been reported yet.

In this study, the lymphatic excretion property of Tm³⁺-doped UCNP was investigated in mice on a long term. Transport and retention of the nanoparticles in lymphatic mapping were evaluated with highly sensitive, high-quality images. Their kinetic luminescence profiles in SLN mapping for injection sites as well as axillary lymph nodes were characterized with *in vivo* quantitative imaging analysis. *Ex vivo* biodistribution of the UCNP was also investigated to confirm their clearance from the lymphatic system.

Results

Hexagonal-phase NaYF₄:Yb³⁺,Tm³⁺ nanocrystals were synthesized with a uniform diameter of approximately 27 nm, as shown in the high-resolution transmission electron microscope (HRTEM) image (Fig. 1a, Supplementary Fig. S1) and X-ray diffraction (XRD) pattern (Supplementary Fig. S2a). The atomic ratio (mol%) of the doped ions was determined as Y:Yb:Tm = 80.9:18.3:0.8 by inductively coupled plasma (ICP) atomic emission spectroscopy analysis. Their upconversion luminescence (UCL) emissions were evaluated at the single particle level with homogeneous and bright NIR emissions around 800 nm from each particle (Fig. 1b,c), which originated from the transition (³H₄ → ³H₆) of activator ions (Tm³⁺) by 980 nm excitation of sensitizer ions (Yb³⁺). These NIR-to-NIR UCL emissions provide highly effective transmissions of excitation and emission lights to deeper areas in the tissues as a biological window for *in vivo* optical imaging^{16,17}.

To improve biocompatibility of UCNP for *in vivo* imaging, the hydrophobic surface was modified by carboxylate functionalized poly(ethylene glycol)-lipid (PEG-lipid) (Supplementary Fig. S2b). The modified UCNP were well dispersed in water and had a mean size of 54 nm and a surface charge of approximately -8 mV as confirmed by dynamic laser scattering (DLS) and zeta potential measurement (Fig. 1d). It was reported that the nanoparticles with a size of around 50 nm show optimal behaviour for transport and retention in lymph node mapping^{18,19}. The negatively charged nanoparticles have advantages for *in vivo* applications because of their relatively less interaction with biological substances, such as proteins or cells with negative surface charges, in blood flow or lymphatic circulation. In particular, they provide less resistance to interstitial transport so that their lymphatic uptake is facilitated^{14,20}. We performed *in vivo* UCL imaging of the lymphatic system in mice using the synthesized UCNP. After injection of a UCNP solution into the forepaw footpad of the mice, UCL emission was detected using a home-built imaging system²¹, which was well designed and suitable for NIR-to-NIR *in vivo* UCL imaging, with extremely low background with minimally residual stray excitation light (Fig. 1e). The lymphatic system rapidly transported the UCNP to SLN through lymphatic flow, and UCL emission from the SLN was clearly detected. After removal of skin, the lymphatic vessel from the injection site to the corresponding SLN was also clearly observed with bright UCL emissions, as shown in Fig. 1f.

To evaluate the SNR of regions of interest (ROIs) in the measured UCL images, two differently sized ROIs were examined as shown in Supplementary Fig. S3. The measured SNR for UCL emission of the lymph node with smaller ROIs was approximately 142 when the power density was under 200 mW/cm², which is 4 times higher than those reported in previous studies¹¹. In the UCL imaging of a small animal, reduction of the overheating effect with 980 nm excitation light should be considered to avoid thermal damage such as burn or fibrosis. In this study, no thermal effect on the animal was observed during UCL imaging, which enables repeated imaging with high temporal resolution in the same animal for a long period, which is consistent with the previous studies⁷. We could also confirm it by hair regrowth after few days at the depilation point for imaging.

Figure 2 shows the *in vivo* temporal behaviour of UCL at the injection site and SLN after the injection. The UCL intensity in SLN indicated a maximum at 4 h post-injection and retained a relatively strong intensity for 4 days. The intensity gradually decreased in SLN as well as at the injection site and was rarely detected at 30 days after the injection. The UCL intensity dropped to approximately 2% at 14 days post-injection compared to that of 4 h post-injection (Supplementary Fig. S4). Note that the measured UCL intensity is totally attributable to the number of UCNP remaining in the ROIs, because there was no photobleaching in the UCNP, and thus no significant signal drop resulted from the UCNP solution for 30 days. We also performed experiment to find the effect of three different surface-functional groups, methoxy-PEG, amine-PEG, and carboxy-PEG (Supplementary Fig. S5). It was observed that the UCL intensity of UCNP functionalized with carboxy-PEG is the largest out of three cases in SLN. However, we could not find any significant difference along them in viewpoint of long-term monitoring.

To further investigate the spatial distribution of the internalized UCNP in the lymph nodes, UCL of the lymph nodes excised from the mice at several time points after the injection was analysed. Figure 3 shows the lymph node stained with haematoxylin and eosin (H&E) and the corresponding UCL images (a) and their magnified high-resolution images (b). At 1 day post-injection, the UCNP were observed mainly in the subcapsular and trabecular sinus regions, whereas the UCNP were rarely detected in deep cortex regions in the lymph node. This suggests that most of the UCNP supplied from the reservoir of footpad were drained out of the lymph node around this time point and did not penetrate the cortex area containing a number of immune cells. At 6 days post-injection, the UCNP were observed relatively in the whole area of the lymph node and were distributed in deeper regions in the lymph node. The UCL intensity at the lymph node was found to be intense for several days after injection, which may be attributed to continuous feeding from the injection site even though the UCNP were drained out of the lymph node. At one month post-injection, the UCNP were rarely found, which suggests that most of the UCNP were excreted from the lymph node. Detailed UCL images of the edge and centre regions of the lymph node are shown in Supplementary Fig. S6.

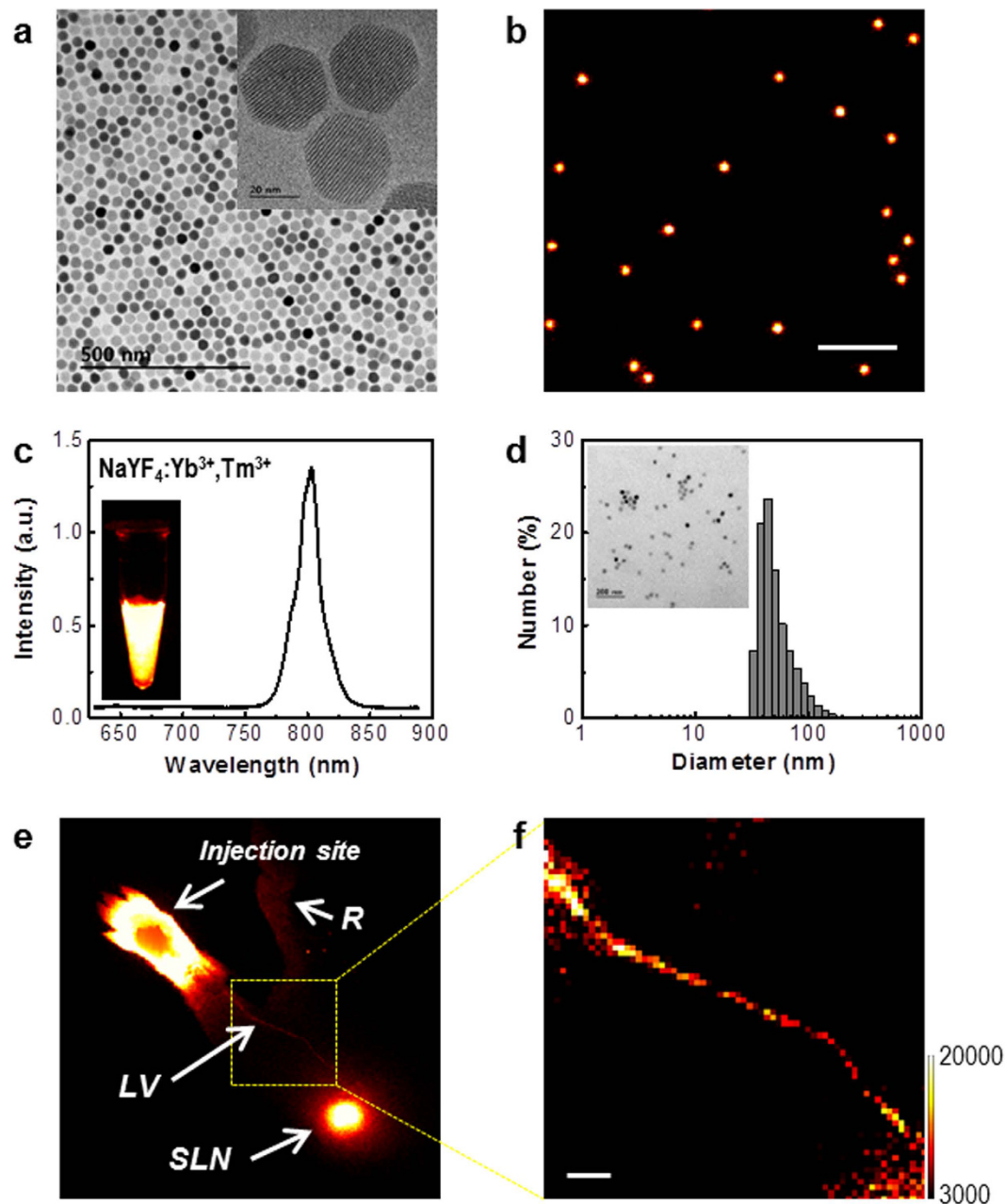


Figure 1. Characterization of the nanocrystals. (a) TEM images of $\text{NaYF}_4:\text{Yb}^{3+}, \text{Tm}^{3+}$ nanocrystals (UCNPs). (b) Single particle upconversion luminescence (UCL) image of the UCNPs. The scale bar is $5\ \mu\text{m}$. (c) UCL spectrum of the UCNPs in organic solvent. (d) Size distribution of the surface-modified and water-soluble UCNPs. The inset shows TEM image of the water-soluble UCNPs. (e) *In vivo* UCL image of mice after injection of the surface-modified UCNPs. LV, lymphatic vessel; SLN, sentinel lymph node; R, reflected secondary emission from the injection site. (f) Magnified UCL image of lymphatic vessel. The scale bar is $1\ \text{mm}$. The size of one pixel is approximately $120 \times 120\ \mu\text{m}$.

To investigate the excretion pathway of the UCNPs, the mice were sacrificed at 1, 6, and 30 days after the injection of UCNPs, and the biodistribution of UCNPs in the mice were observed by UCL imaging. According to the UCL images shown in Fig. 4a, the UCNPs were found mainly in the liver and spleen at 1 day post-injection, whereas they were not detected in other organs. The signal intensity in the organs decreased at 6 days post-injection. The UCNPs were rarely detected in any organs at 30 days post-injection. Faeces from the mice were collected daily and imaged after the injection, as indicated in Fig. 4b. The UCNPs were found for the first week after the injection but no longer detected at 30 days post-injection. In accordance with the distribution changes in the lymph node, it was considered that the UCNPs were excreted by the blood circulation system through accumulation in liver and spleen following lymphatic drainage. It has been reported that molecules taken in by the lymphatic system are transported to the system circulation via the thoracic duct and subclavian

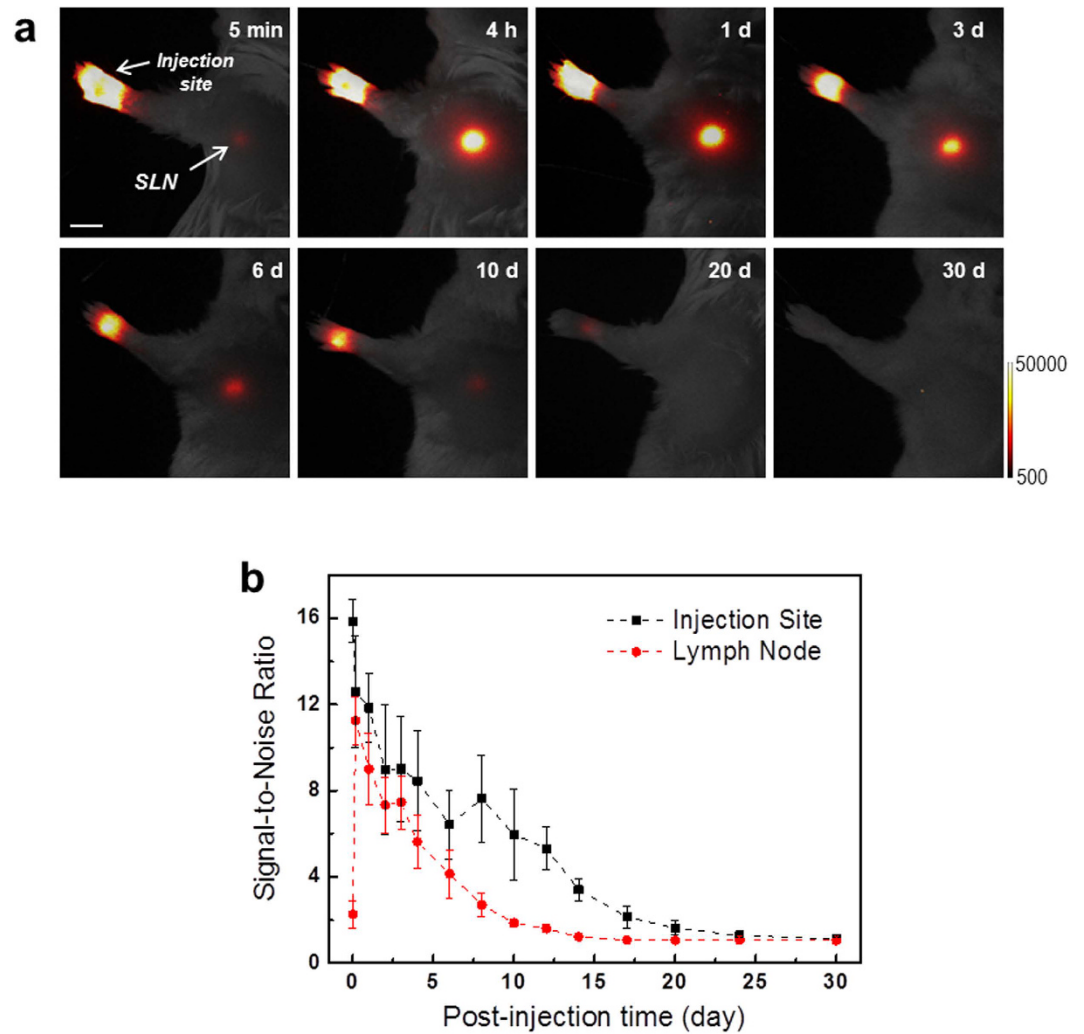


Figure 2. *In vivo* temporal behaviour of UCL. (a) *In vivo* UCL imaging of lymph node in the same mouse at different post-injection times. Mice were subcutaneously injected in the forepaw footpad with the UCNPs. The scale bar is 5 mm. (b) Comparison of time-dependent signal-to-noise ratio values of UCL signals between the injection site and axillary lymph node of mice ($N = 4$).

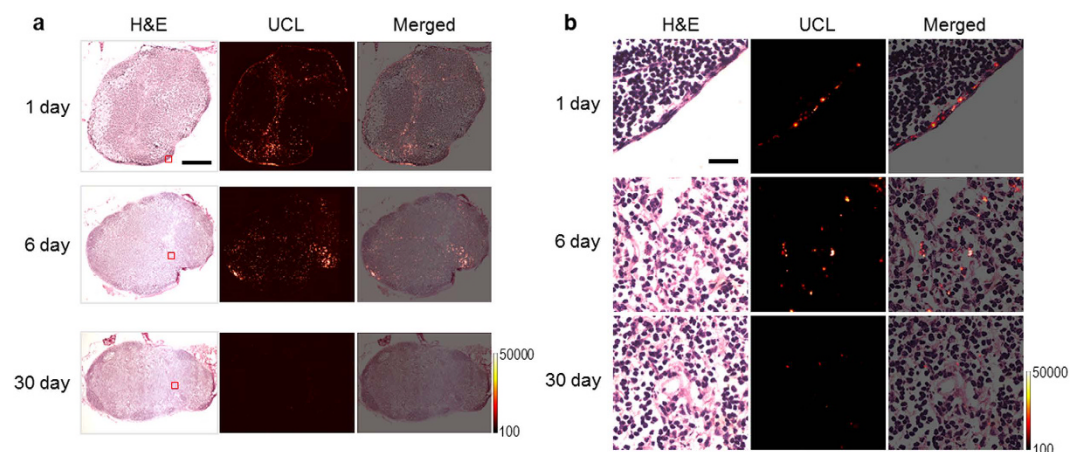


Figure 3. Spatial distribution of the internalized UCNPs in the lymph nodes. (a) H&E staining and corresponding UCL images of dissected axillary lymph nodes from the mice treated with UCNPs. The lymph nodes were obtained on 1, 6, and 30 days after the injections. The scale bar is 0.5 mm. (b) Magnified images of the areas marked by red rectangles in (a). The scale bar is 30 μm .

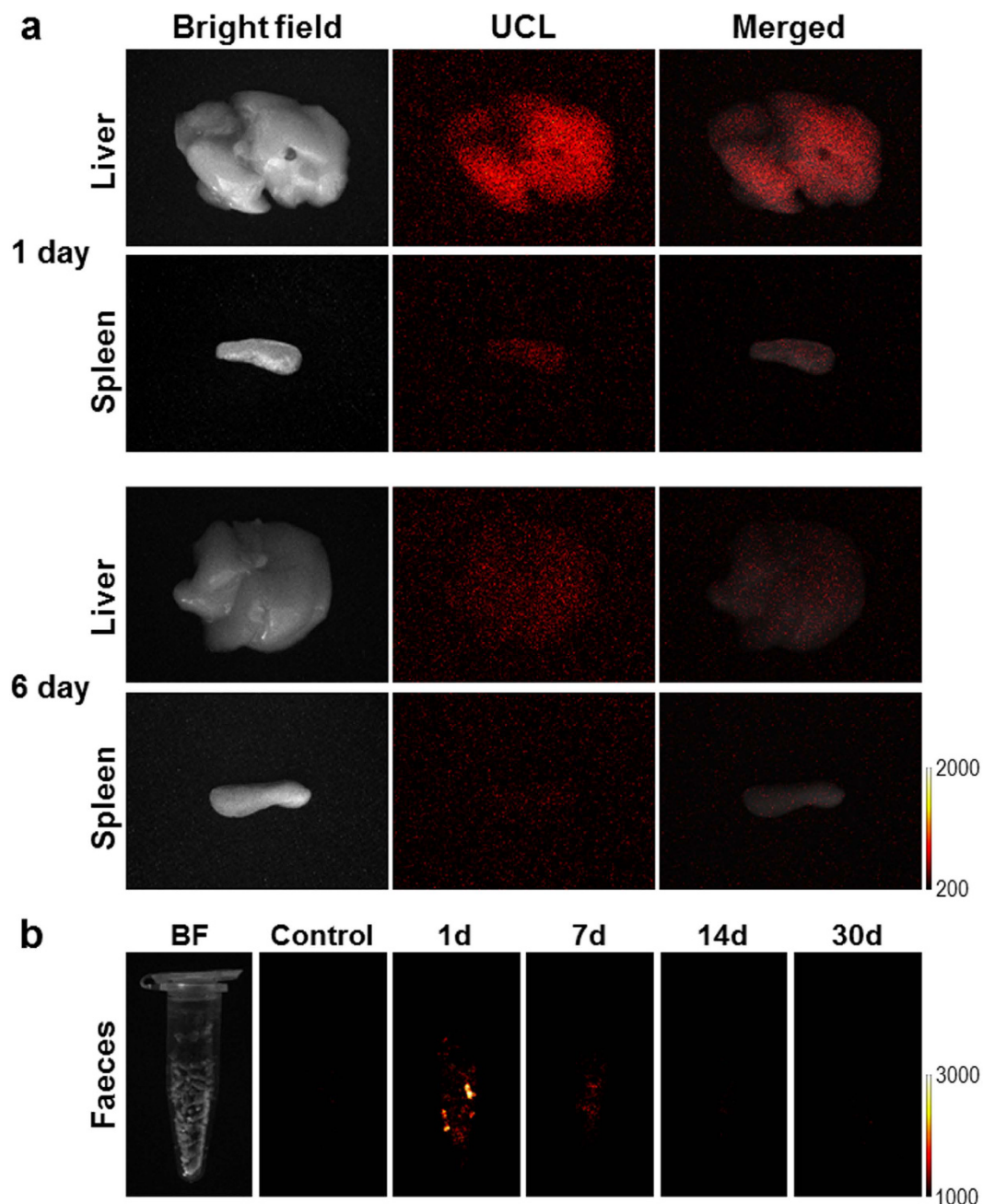


Figure 4. *Ex vivo* imaging of UCL from the mice. (a) *Ex vivo* UCL images of the major organs obtained from the mice after injection of the surface modified UCNPs at different post-injection times. (b) UCL images of the faeces from the mice.

veins^{22,23}. Recently, biodistribution studies of UCNPs after intravenous injection in mice have reported clear excretion of UCNPs through the hepatobiliary pathway^{21,24}. Here, we speculate that the subcutaneously injected UCNPs could be efficiently excreted through the hepatobiliary route in mice for up to 1 month post-injection.

In summary, we synthesized highly uniform and biocompatible Tm^{3+} -doped UCNPs optimized for long-term *in vivo* imaging. It was observed that the UCNPs injected into the forepaw footpad of the mice were transported rapidly to the SLN and accumulated in the SLN for 3–4 days. According to the biodistribution the injected UCNPs were transported from the lymphatic system to the blood stream and eventually excreted in approximately 1 month post-injection. These results suggest potential applications of UCNPs with high-quality images for non-invasive, quantitative long-term *in vivo* optical imaging in the biological and medical fields, especially in biochemistry with applications in metastatic tumour detection in lymph node or in *in vivo* image-tracking of the UCNP-labelled immune cells for cell therapy.

Methods

Chemicals. $\text{YCl}_3 \cdot 6\text{H}_2\text{O}$ (99.99%), $\text{YbCl}_3 \cdot 6\text{H}_2\text{O}$ (99.9%), TmCl_3 (99.9%), oleic acid ($\geq 99\%$), 1-octadecene ($\geq 95.0\%$), sodium hydroxide (97%), and ammonium fluoride ($\geq 98\%$) were purchased from Sigma-Aldrich and used without further purification. 1,2-distearoyl-*sn*-glycero-3-phosphoethanolamine-N-[carboxy(polyethylene glycol)-2000] (DSPE-PEG-COOH) was purchased from Nanocs Inc. (New York, NY, USA).

Synthesis of hexagonal-phase $\text{NaYF}_4:\text{Yb}^{3+},\text{Tm}^{3+}$ nanoparticles. Hexagonal-phase UCNPs were synthesized using previously reported methods²⁵. Y-oleate (0.79 mmol), Yb-oleate (0.20 mmol), and Tm-oleate (0.01 mmol) complexes were mixed with oleic acid (8 ml) and 1-octadecene (15 ml) in a 100 ml three-neck round bottom flask under vacuum for 30 min. The mixture was heated to 100 °C under vacuum with stirring for 30 min and then cooled to room temperature under Ar atmosphere. NaOH (2.5 mmol) and NH_4F (4 mmol) dissolved in methanol (10 ml) were slowly added to the reaction mixture under Ar atmosphere at 50 °C. The mixture was heated to 100 °C under vacuum with stirring for 30 min until residual methanol was completely removed. Subsequently, it was heated to 300 °C at a constant heating rate of 3.3 °C/min and kept at that temperature for 1.5 h under Ar atmosphere. After cooling down to room temperature, UCNPs were precipitated by adding excess ethanol and isolated by centrifugation performed 3 times. The purified UCNPs were dispersed in hexane.

Surface modification of nanoparticles by carboxylic acid functionalized phospholipid-PEG. 1 mg of UCNPs was dispersed in 100 μl of chloroform. 10 mg of DSPE-PEG-COOH was dispersed in water in a sonication bath for 30 min. UCNP solution was slowly added to lipid solution during tip sonication (Branson Sonifier, Danbury, USA). The emulsion was vigorously vortexed for 5 min and stirred until residual chloroform was completely removed. The surface-modified UCNPs were purified by centrifugation and dispersed in water.

Characterization of nanoparticles. The synthesized nanoparticles were characterized by HRTEM and XRD. TEM images were obtained on a Philips Tecnai F20 electron microscope, and the XRD pattern was produced on a Bruker AXS (D8 DISCOVER) instrument equipped with Cu K_α radiation ($\lambda = 1.5418 \text{ \AA}$). Particle size distribution and surface zeta potential were analysed on a Zetasizer Nano ZS instrument (Malvern Instruments, Malvern, UK). Elemental analysis of nanoparticles was performed by ICP optical emission spectroscopy (Optima 8300DV or 4300DV, Perkin Elmer, Waltham, MA, USA).

Measurement of the upconversion luminescence spectra and images of UCNPs. The UCNP solutions were excited by a 980 nm continuous-wave (CW) single-mode diode laser (P161-600-980A, EM4, Andor Technology, Belfast, UK). Their emission was collected through an optical fibre by a home-made UCL spectrograph and imaging system, which was composed of an inverted microscope (IX71, Olympus, Tokyo, Japan) and an electron multiplying charge coupled device (EMCCD) camera (DV897DCS-BV, iXon, Andor Technology, Belfast, UK). It was detected by a CCD camera (PIXIS 400BR, Princeton Instruments, Trenton, NJ, USA) attached to an imaging spectrograph (IsoPlane SCT320, Princeton Instruments). The images of individual UCNPs or UCNPs in sliced SLN tissues were taken from the same imaging system. To obtain colour images of SLN tissues, a colour sCMOS camera (OS4MPc-CL-RGB, Raptor Photonics, Larne, UK) was employed.

In vivo and ex vivo UCL imaging. Male BALB/c mice (6 weeks of age) were purchased from OrientBio (Kyunggi-do, Korea), and the imaging areas were treated with a depilatory cream. Surface-modified UCNP solution (20 μl of 25 pM) was injected subcutaneously into the forepaw footpad. To supply homogeneous nanoparticles to the animals, we injected the particles right after removing the aggregates by syringe filtration with a correction of its concentration. Then the mice ($n = 4$) were placed in a home-made high-quality UCL *in vivo* imaging system connected to an EMCCD camera (DU897-EX, iXon Ultra, Andor Technology). UCL images of mice were acquired using a high-power (0–30 W) 980 nm diode laser (Dilas, Lysyn Yepli, Bucheon, Korea) as an excitation light source and two emission filters (FF01-800/12 and FF01-890/SP, Semrock, Rochester, NY, USA). All images were processed with the Andor Solis software (Andor Technology, Belfast, UK).

This *in vivo* study followed the guidelines of the committee on animal research at the Korea Basic Science Institute (KBSI), with the protocol approved by the local institutional review committee on animal care (KBSI-AEC1508). For the imaging of organs and faeces, the mice ($n = 3$) were sacrificed at different post-injection times and the organs (axillary lymph node, heart, lungs, kidneys, liver, stomach, spleen, intestine, and injection site) were removed and imaged using the UCL imaging system. The faeces were collected daily for the first 7 days and at 10, 14, 22, and 30 days after injection. The mice were housed in a metabolic cage to collect faeces.

Histologic analysis. To analyse *in situ* distribution of UCNPs, three groups of the mice ($n = 3$ per group) were sacrificed on 1, 6 and 30 days, and then axillary lymph nodes were dissected and embedded in a Tissue-Tek OCT compound (Sakura, Tokyo, Japan) and frozen in liquid nitrogen. Cryosections ($\sim 8 \mu\text{m}$) were prepared by a cryostatic microtome (Leica Microsystems Nussloch GmbH, Nussloch, Germany) and were transferred to glass slides and stained with hematoxylin and eosin (H&E).

References

1. Cochran, A. J. *et al.* Tumour-induced immune modulation of sentinel lymph nodes. *Nat. Rev. Immunol.* **6**, 659–670 (2006).
2. von Andrian, U. H. & Mempel, T. R. Homing and cellular traffic in lymph nodes. *Nat. Rev. Immunol.* **3**, 867–878 (2003).
3. Jain, R., Dandekar, P. & Patravale, V. Diagnostic nanocarriers for sentinel lymph node imaging. *J. Control. Release* **138**, 90–102 (2009).
4. Niu, G. & Chen, X. Lymphatic imaging: Focus on imaging probes. *Theranostics* **5**, 686–697 (2015).
5. Noh, Y.-W. *et al.* Near-infrared emitting polymer nanogels for efficient sentinel lymph node mapping. *ACS Nano* **6**, 7820–7831 (2012).
6. Kim, S. *et al.* Near-infrared fluorescent type II quantum dots for sentinel lymph node mapping. *Nat. Biotechnol.* **22**, 93–97 (2004).

7. Zhou, J., Liu, Z. & Li, F. Upconversion nanophosphors for small-animal imaging. *Chem. Soc. Rev.* **41**, 1323–1349 (2012).
8. Sun, Y., Feng, W., Yang, P., Huang, C. & Li, F. The biosafety of lanthanide upconversion nanomaterials. *Chem. Soc. Rev.* **44**, 1509–1525 (2015).
9. Wang, F. & Liu, X. Recent advances in the chemistry of lanthanide-doped upconversion nanocrystals. *Chem. Soc. Rev.* **38**, 976–989 (2009).
10. Zhou, J., Liu, Q., Sun, Y. & Li, F. Upconversion luminescent materials: Advances and applications. *Chem. Rev.* **115**, 395–465 (2015).
11. Cao, T. *et al.* High-quality water-soluble and surface-functionalized upconversion nanocrystals as luminescent probes for bioimaging. *Biomaterials* **32**, 2959–2968 (2011).
12. Cheng, L. *et al.* Highly-sensitive multiplexed *in vivo* imaging using PEGylated upconversion nanoparticles. *Nano Res.* **3**, 722–732 (2010).
13. Kobayashi, H. *et al.* *In vivo* multiple color lymphatic imaging using upconverting nanocrystals. *J. Mater. Chem.* **19**, 6481–6484 (2009).
14. Helle, M. *et al.* Surface chemistry architecture of silica nanoparticles determine the efficiency of *in vivo* fluorescence lymph node mapping. *ACS Nano* **7**, 8645–8657 (2013).
15. Fu, C. *et al.* The absorption, distribution, excretion and toxicity of mesoporous silica nanoparticles in mice following different exposure routes. *Biomaterials* **34**, 2565–2575 (2013).
16. Nyk, M., Kumar, R., Ohulchanskyy, T. Y., Bergey, E. J. & Prasad, P. N. High contrast *in vitro* and *in vivo* photoluminescence bioimaging using near infrared to near infrared up-conversion in Tm^{3+} and Yb^{3+} doped fluoride nanophosphors. *Nano Lett.* **8**, 3834–3838 (2008).
17. Xia, A. *et al.* Core-shell $\text{NaYF}_4:\text{Yb}^{3+}, \text{Tm}^{3+} @ \text{Fe}_3\text{O}_4$ nanocrystals for dual-modality T_2 -enhanced magnetic resonance and NIR-to-NIR upconversion luminescence imaging of small-animal lymphatic node. *Biomaterials* **32**, 7200–7208 (2011).
18. Cai, X. *et al.* *In vivo* quantitative evaluation of the transport kinetics of gold nanocages in a lymphatic system by noninvasive photoacoustic tomography. *ACS Nano* **5**, 9658–9667 (2011).
19. Khullar, O., Frangioni, J. V., Grinstaff, M. & Colson, Y. L. Image-guided sentinel lymph node mapping and nanotechnology-based nodal treatment in lung cancer using invisible near-infrared fluorescent light. *Semin. Thorac. Cardiovasc. Surg.* **21**, 309–315 (2009).
20. Swartz, M. A. The physiology of the lymphatic system. *Adv. Drug Deliver. Rev.* **50**, 3–20 (2001).
21. Seo, H. J. *et al.* Rapid hepatobiliary excretion of micelle-encapsulated/radiolabeled upconverting nanoparticles as an integrated form. *Sci. Rep.* **5**, 15685 (2015).
22. Zou, Y. *et al.* Lymphatic absorption, metabolism, and excretion of a therapeutic peptide in dogs and rats. *Drug Metab. Dispos.* **41**, 2206–2214 (2013).
23. McDonald, T. A., Zepeda, M. L., Tomlinson, M. J., Bee, W. H. & Ivens, I. A. Subcutaneous administration of biotherapeutics: Current experience in animal models. *Curr. Opin. Mol. Ther.* **12**, 461–470 (2010).
24. Xiong, L., Yang, T., Yang, Y., Xu, C. & Li, F. Long-term *in vivo* biodistribution imaging and toxicity of polyacrylic acid-coated upconversion nanophosphors. *Biomaterials* **31**, 7078–7085 (2010).
25. Li, Z. & Zhang, Y. An efficient and user-friendly method for the synthesis of hexagonal-phase $\text{NaYF}_4:\text{Yb}$, Er/Tm nanocrystals with controllable shape and upconversion fluorescence. *Nanotechnology* **19**, 345606 (2008).

Acknowledgements

This work was supported by a grant (K.S.H., D36401) from the Korea Basic Science Institute, the R&D Convergence Program (K.S.H., CRC-15-02-KRIBB), the CAP (K.S.H., PBF050), the DRC Program (Y.D.S., 2014) funded by the Korea National Research Council of Science and Technology, and by a grant (Y.D.S., SI1509) from the Korea Research Institute of Chemical Technology.

Author Contributions

H.S.P. and S.H.N. designed the study, performed experiments, analysed data and wrote the manuscript. J.K. assisted with *in vivo* optical imaging. H.S.S. performed experiments on biodistribution and analysed the data by ICP-AES. K.S.H. and Y.D.S. directed the project, designed the experiments, analysed the data and wrote the manuscript. All authors discussed the results and commented on the manuscript.

Additional Information

Supplementary information accompanies this paper at <http://www.nature.com/srep>

Competing financial interests: The authors declare no competing financial interests.

How to cite this article: Park, H. S. *et al.* Clear-cut observation of clearance of sustainable upconverting nanoparticles from lymphatic system of small living mice. *Sci. Rep.* **6**, 27407; doi: 10.1038/srep27407 (2016).



This work is licensed under a Creative Commons Attribution 4.0 International License. The images or other third party material in this article are included in the article's Creative Commons license, unless indicated otherwise in the credit line; if the material is not included under the Creative Commons license, users will need to obtain permission from the license holder to reproduce the material. To view a copy of this license, visit <http://creativecommons.org/licenses/by/4.0/>